Computer Modeling of Bevacizumab Drug Distribution After Intravitreal Injection in Rabbit and Human Eyes

Jabia M. Chowdhury[a,b], Eduardo A. Chacin Ruiz[a], Katelyn E. Swindle-Reilly[c,d,e], Ashlee N. Ford Versypt[a,f,g,*]

[a]*Department of Chemical and Biological Engineering, University at Buffalo, The State University of New York, Buffalo, NY, 14260, USA*
[b]*Department of Electrical Engineering, Texas A&M University-Texarkana, Texarkana, TX, 75503, USA*
[c]*Department of Biomedical Engineering, The Ohio State University, Columbus, OH, 43210, USA*
[d]*William G. Lowrie Department of Chemical and Biomolecular Engineering, The Ohio State University, Columbus, OH, 43210, USA*
[e]*Department of Ophthalmology and Visual Sciences, The Ohio State University, Columbus, OH, 43212, USA*
[f]*Department of Biomedical Engineering, University at Buffalo, The State University of New York, Buffalo, NY, 14260, USA*
[g]*Institute for Artificial Intelligence and Data Science, University at Buffalo, The State University of New York, Buffalo, NY, 14260, USA*

Abstract

Age-related macular degeneration (AMD) is a condition brought on by macular deterioration caused primarily by inflammation and cell death in the retina. There is no cure for the disease and current treatments for advanced (wet) AMD rely on intravitreal injections of anti-vascular endothelial growth factor (anti-VEGF) therapeutics. One common off-label anti-VEGF drug used in AMD treatment is bevacizumab. There have been experimental efforts to investigate the pharmacokinetic (PK) behavior of bevacizumab in the vitreous and aqueous humor. Still the quantitative effect of elimination routes and drug concentration in the macula are not well understood. In our study, we developed two spatial models representing rabbit and human vitreous humor to better understand the PK behavior of bevacizumab. We explored convective effects on the vitreous while considering the anterior elimination alone or coupled with posterior elimination. We compared our models with available experimental data and calculated an approximate macula concentration. Our results show that both anterior and posterior elimination play a role in bevacizumab clearance from the eye. Furthermore, an effective bevacizumab concentration close to the macula region is maintained for shorter time periods when compared to the whole vitreous region. This model can improve knowledge and understanding of AMD treatment.

Keywords: ocular pharmacokinetics, ophthalmic drug distribution, age-related macular degeneration, anti-VEGF, mass transport, COMSOL, vitreous humor, elimination routes

*Corresponding author at: 507 Furnas Hall, University at Buffalo, The State University of New York, Buffalo, NY 14260. Email address: ashleefv@buffalo.edu

1. Introduction

Retinal diseases are considered the most common cause of vision loss in all age groups. The retina, including the macula, is located in the posterior segment of the eye and consists of several layers of cells. The macula is positioned at the retina's center and is responsible for visual clarity. Hypoxia occurs when a cell receives less oxygen than required, and this condition can cause vascular endothelial cell growth factor expression. At the macula, this promotes the formation of aberrant new blood vessels, causing the irremediable wet form of age-related macular degeneration (AMD). AMD damages the macula and affects the center of the visual field, which limits the patient's ability to see clearly.

In the United States, around 11 million people suffer from AMD [1, 2], which is expected to double to 22 million by 2050 [3]. AMD is generally found in people older than 65 years [4, 5]. AMD is an irreversible disease that can cause complete vision loss if it is not treated in time. Early detection of AMD could reduce the visual impairment of the patient. There are two types of AMD: non-neovascular (dry) AMD and neovascular (wet) AMD. The most common AMD is dry AMD, which refers to the early stages of the disease when drusen deposition and possible geographic atrophy of the macula occur [6]. Dry AMD at any stage can turn into wet AMD. Wet AMD is caused by abnormal blood vessel growth under the retina, and it causes severe vision loss due to overproduction of vascular endothelial growth factor (VEGF) [7].

VEGF is a protein that is essential in the growth of blood vessels. VEGF signals for promoting new blood vessel production while facing hypoxic conditions. The overproduction of VEGF causes the disordered growth of new blood vessels in the macula. Therefore, anti-VEGF therapeutics are widely accepted to treat retinal neovascular diseases like AMD. The five most commonly used anti-VEGF therapeutics used in AMD treatment are approved by the US Food and Drug Administration (FDA) [8]. Several ocular therapeutic approaches including intravitreal injection, drug implant, laser photocoagulation, and photodynamic therapy have been used to treat retinal diseases like AMD. Intravitreal injection of anti-VEGF drugs is considered the most common option in AMD treatment [9] since it allows high drug concentration to the retinal layer with minimal side effects from the localized ocular treatment that can be performed in-office. In this work, one of the most readily available and commonly used anti-VEGF therapeutics, bevacizumab (Avastin), is considered in our computational drug distribution model to investigate its PK in the vitreous humor and penetration to the macula.

Several experiments have been done to investigate the PK of the drug bevacizumab in animal models [10, 11, 12]. Less emphasis has been placed on developing a physiologically based PK model in the eye for bevacizumab [13]. One research study analyzed an *in silico* model of bevacizumab release from intravitreally delivered drug-loaded PLGA microspheres and observed the drug distribution profile [14]. The limitation of this work is the drug diffusion coefficient used in the simulation was not for the drug bevacizumab but for fluorescein. The drug bevacizumab's molecular weight (MW) is 149 kDa, and fluorescein has an MW of 0.332 Da, three orders of magnitude smaller. Since bevacizumab is a much larger drug than fluorescein, the value of the drug

diffusion coefficient for fluorescein is not representative of bevacizumab. This work included bevacizumab release from intravitreally administrated PLGA microspheres whereas, in our model, we consider intravitreal injection directly.

Sibak et al. [15] studied heat, momentum, and and mass transport in a 3D eye model after intravitreal injection of bevacizumab. They considered a simplified form of the Navier-Stokes equation for momentum transport. For mass transport, they considered diffusion-convection in the aqueous humor and diffusion only in the vitreous humor. Intravitreal injection was modeled as an instantaneous point source. Their boundary conditions included concentration zero at the iris and choroid. In our model, we focus on the vitreous humor only, with a clinically relevant injection of volume 0.05 mL. Our boundary conditions are at the lens and the choroid, but the conditions imposed change based on cases discussed later for considering anterior elimination alone or in combination with posterior routes of elimination.

Hutton-Smith et al. [16] published a mechanistic model of intravitreal PK and pharmacodynamic aspects of using ranibizumab for AMD treatment. Our current work is not similar to their research goal, as their primary focus was to capture the response of the drug reducing the ocular VEGRF in patients besides the PK effect using a two-compartmental model. Their *in vivo* PK studies focused on calculating ocular half-life for various drugs in animal species data. In our work, we observe the drug's PK effect, measure the drug bevacizumab concentration near the macula region, and observe the duration of the required amount of drug present at that location. Our model is the first known computational model that simultaneously studies the PK effect of intravitreally injected bevacizumab in both human and rabbit eyes and also calculates the time-concentration plot near the macula region.

In AMD treatment, the target of the therapeutics is to control the abnormal cell/blood vessel growth in the macula. The most frequently used delivery mechanism for these treatments for AMD is intravitreal injections. Drug transport to the retinal layer depends on the anatomical properties of the vitreous in the eye. Different investigations have been done to simulate the vitreous humor region. Khoobyar et al. [17] considered the vitreous humor as a porous media and divided the vitreous into a low permeability (gel) and high permeability (liquid) region described by the Darcy flow. However, this subdivision of the vitreous humor into a gel and a liquid region, while physiologically relevant, still needs more investigation. Balachandran [18] considered the vitreous motion and mode of vitreous humor using a saccade-induced flow field. Researchers noticed that the degree of liquefaction was correlated with an increase in vitreous mobility caused by fast ocular oscillations. Ocular oscillations, also known as saccades, assist in orienting the line of sight and enable us to concentrate at various locations regularly. Rapid saccades may cause the vitreous to swirl at high speeds, leading to considerable convective transfer. Including ocular oscillations in the model made numerical solutions more difficult as the fluid flow field became more complex, and the model did not perform well at low viscosity. Brinkman's equation is another way to solve the porous media, and it was used by Khoobyar et al. [19] while solving the computational analysis of the vitreous humor and used Darcy's law analytically to solve their model. The vitreous humor is a gel-like porous structure, and the fluid that transports through the vitreous is accurately described using Darcy's law. The researcher used Darcy's law and Brinkman's equation to implement the

fluid flow and momentum transport equations in the vitreous humor.

In this work, we developed a time-dependent, three-dimensional model for intravitreal drug delivery in the posterior segment of the eye, specifically in the vitreous humor. We used the recombinant humanized monoclonal antibody bevacizumab. Our goal of using this injected anti-VEGF agent into the vitreous humor is to observe the drug concentration both at the vitreous humor and near the target location, the macula, for the full form of the antibody. We studied the PK effect of the drug and validated the time-concentration plot in the vitreous with the experimental PK results taken from rabbit and human eyes. In our model, we estimated the drug concentration near the macula region in both rabbit and human eyes after an intravitreal injection and determined the number of days where VEGF is expected to be completely inhibited.

2. Methods

A PK study is used to evaluate the concentration profile of bevacizumab by considering the processes of absorption, distribution, metabolism, and excretion (ADME). Although PK models utilizing the anti-VEGF medication bevacizumab have seen very little research [15], several experimental PK models using rabbit eyes [10, 20, 21, 22] and one experimental PK model using human eyes [23] are available.

In our study, we created a 3D spherical geometry of the vitreous humor surrounded by the hyaloid membrane, lens, and the outer surface of the vitreous, which is attached to the retinal layer (Figure 1a). Drug transport was modeled using a convection-diffusion equation coupled with the velocity profile obtained from Darcy's law in the porous domain. The drug transport through the vitreous is solved using the transport of diluted species physics in COMSOL. Our computational PK model does not include the effect of metabolism and degradation of bevacizumab as it is negligible in the eye [24].

We simulated a standard dose (1.25mg/0.05mL) of bevacizumab used in patients. This drug is injected intravitreally behind the surgical limbus using a 30-gauge needle [10], which is the most common injected position applied in most of the experimental studies.

In our 3D model, we estimated the concentration of bevacizumab in the vitreous and the macula region. In our geometry, as we did not include the retinal layer; instead, we fixed a point at the boundary of the outer vitreous and defined it as the near the macula region (Figure 1a). At this point, we calculated either drug concentration or drug flux depending on the case. We collected data from previously performed experimental studies from rabbit and human eye models to validate our model. These experiments were done following a similar methodology. Briefly, 1.25 mg/0.05 mL of bevacizumab was injected near the limbus region in the vitreous using 30-gauge needles. Our simulations are performed under the same conditions as these experiments. The data were collected from prior publications using WebPlotDigitizer [25]. We did not find any experimental data measuring drug concentration at the macula in human eyes or at the visual streak in rabbit eyes. To control the endothelial cell growth to inhibit VEGF completely, the minimum concentration of the therapeutic antibody bevacizumab needs to be 500 ng/mL (0.5 μg/mL) [26]. We determined

the number of days when the bevacizumab concentration was above this threshold near the macula location. Figure 1 includes the 3D figure of the geometric model and the boundary conditions.

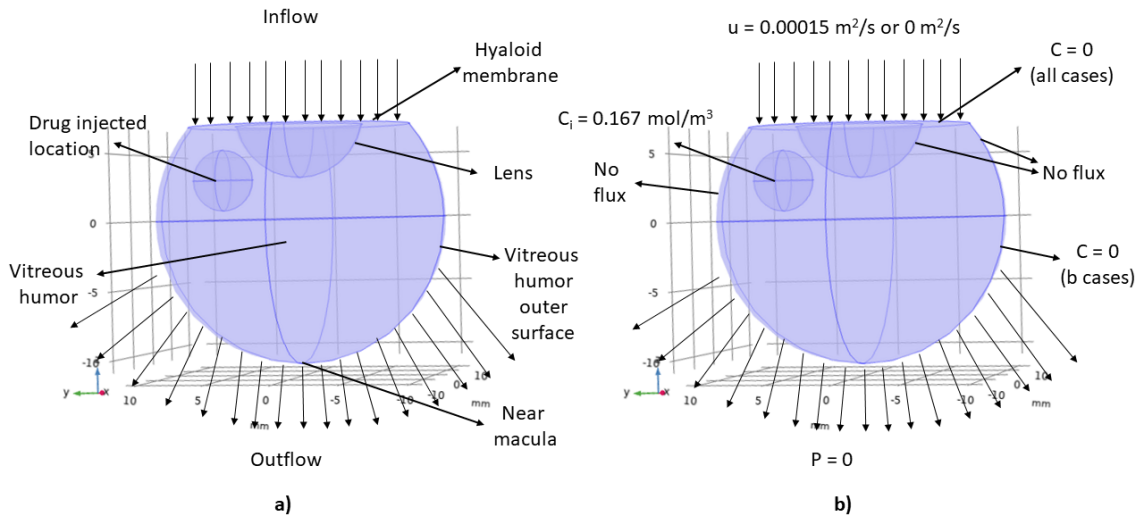

Figure 1: 3D geometry of the eye. a) Anatomy description b) Boundary conditions

2.1. Geometry

The biggest difference between the rabbit and human vitreous humor is the size. The human vitreous is approximately three times bigger than the rabbit vitreous. The vitreous volume in rabbit eyes varies from 1.15 to 1.7 mL [27]. The shapes of both our models are influenced by the geometry from Khoobyar et al. [17]. The human vitreous is larger, and its volume range varies between 4.22 and 5.43 mL [28]. In the models by Missel [29], the rabbit and human vitreous humor were set as 1.52 and 4.85 mL, respectively.

We have created a three-dimensional geometry of the vitreous humor for rabbit and human eyes. The vitreous humor's shape is considered spherical in our model. The vitreous is located in the 3D domain with its origin at $(x,y,z) = (0,0,0)$ mm and a radius of 7.6 mm for rabbit vitreous and 10.9 mm for human vitreous. We used a volume of 1.44 mL for the rabbit vitreous and 4.79 mL for the human vitreous. The injection shape is considered a sphere with a volume of 0.05 mL. The injected location is near the limbus region where the coordinates are $(x,y,z) = (0,4.9,-3.5)$ mm for the rabbit vitreous and $(x,y,z) = (0,6,3)$ mm for the human vitreous. As previously mentioned, the target of the therapeutic bevacizumab is the macula region, located in the middle of the retina and attached to the outer boundary of the vitreous in our model. Table 1 summarizes the geometry properties in our model.

Table 1: Parameter values for eye geometries

Parameter	**Rabbit**	**Human**	**Unit**
Vitreous humor origin (x_v, y_v, z_v)	(0, 0 , 0)	(0, 0 , 0)	m
Vitreous humor radius r_v	7.60×10^{-3}	10.90×10^{-3}	m
Vitreous humor volume	1.44×10^{-6}	4.79×10^{-6}	m^3
Lens origin (x_l, y_l, z_l)	$(0, 0 , 4)\times10^{-3}$	$(0, 0 , 8)\times10^{-3}$	m
Lens radius r_l	4.00×10^{-3}	4.90×10^{-3}	m
Injection origin (x_i, y_i, z_i)	$(0, 4.9, -0.3)\times10^{-3}$	$(0, 6, 3)\times10^{-3}$	m
Injection radius r_i	2.30×10^{-3}	2.30×10^{-3}	m
Near macula location (x_m, y_m, $z_m = -r_v$)	$(0, 0, -7.60)\times10^{-3}$	$(0, 0, -10.90)\times10^{-3}$	m

The other three tissues–retina, lens, and hyaloid membrane–are bounded around the vitreous humor, which is considered in our geometry and is shown in Figure 1a. Figure 1b shows the boundary conditions of the geometrical model. We created our geometry in COMSOL 6.1 and used an extra fine, physics-controlled mesh.

2.2. Modeling of the vitreous humor

The vitreous humor has viscoelastic properties and is a colorless, transparent, gel-like material that contains 99% of water [30, 31]. The vitreous humor is located at the center of the eye, between the lens and the retina and covers 80% of the eye volume [32]. The vitreous humor maintains the shape and size of the eye and protects the retina from any disturbing substances as the vitreous humor is rigidly attached to some regions of the retina. Treatment of inner retinal diseases is challenging because of the anatomical complexity of the posterior segment of the eye. The healthy young vitreous is an intact viscoelastic gel-like material that liquefies with age [32]. The vitreous fluid is responsible for preventing bulk movements of solute.

We have applied a no-flux boundary condition at the lens surface as it is impermeable to water and drugs. The no-flux boundary condition is defined by

$$-\mathbf{n} \cdot \rho u = 0 \tag{1}$$

where n is the unit normal vector, ρ is the density, and u is the fluid velocity.

Considering the vitreous humor structural properties, we have investigated two cases in our model.

Case 1: We consider the vitreous humor as a porous structure and simulate the vitreous humor as a porous viscoelastic material. The aqueous humor fluid produced from the ciliary body enters the vitreous cavity through the retrozonular and retrolental spaces [33]. The aqueous humor permeates the vitreous through the hyaloid membrane, and we considered it as an inlet fluid velocity in our model (Figure 1). We assumed that aqueous humor fluid moves through the vitreous humor. A reference pressure of 0 Pa was set at the outflow boundary condition (Figure 1).

Previous studies used different approaches to solve the vitreous humor simulation in computational drug delivery models. Brinkman's equation and Darcy's law are two common methods used to simulate the vitreous humor as a porous structure. We considered the aqueous fluid coming through the hyaloid membrane with the inlet velocity of 0.00015 mm/s and solved for Darcy's law. In this simulation, we considered convective flow due to the aqueous fluid presence in the vitreous, porous domain, influenced by Khoobyar et al. [17]. In our model, the vitreous humor is considered a porous structure with a porosity value of $\varepsilon = 1$ [34].

The governing equation used in Darcy's law is given by

$$u = \left(\frac{\kappa}{\mu}\right) \nabla p \tag{2}$$

$$\frac{\partial}{\partial t}(\rho\varepsilon) + \nabla \cdot (\rho u) = Q_m \tag{3}$$

where u is Darcy's velocity, κ is the permeability of the vitreous, μ is the dynamic viscosity of the aqueous humor, p is the aqueous humor pressure, ρ is the density of the aqueous humor, ε is the porosity, and Q_m is the mass source term. In COMSOL, these parameters are used to define the vitreous material properties. Darcy's law's initial condition is zero for all boundaries ($p = 0$). Table 2 includes all the parameters used to define Darcy's law.

Case 2: It is commonly assumed that the fluid in the vitreous is "stagnant" when modeling transport across the vitreous humor [29, 35]. In this Case, we consider zero inlet velocity ($u = 0$) in the vitreous humor meaning there is no convective flow in the vitreous.

Furthermore, a recent study observed the elimination routes of anti-VEGF therapeutics in both human and rabbit vitreous [24]. The results suggested that the anterior elimination route is dominant compared to the posterior route for bevacizumab and other anti-VEGF drugs in both human and rabbit eyes. This dominance is dependent on the aqueous humor flow rate in the eye. In our simulation, we considered two elimination routes: Case a: only anterior elimination, and Case b: both anterior and posterior elimination. A more thorough explanation of these two cases is given in the next section. We did not consider a posterior elimination route alone, given that the intravitreal injections are administered behind the surgical limbus, which is significantly closer to the anterior eye segment.

We combined the two cases for convective flow modeling in the vitreous humor with the two elimination cases for a total of four case studies. We studied convective flow in the vitreous with anterior elimination only (Case 1a), convective flow with both anterior and posterior elimination (Case 1b), no convective flow with anterior elimination (Case 2a), and no convective flow with both anterior and posterior elimination (Case 2b). We compared our predicted bevacizumab concentration in the vitreous with the experimental data for both human and rabbit eyes. We also estimated drug concentration near the macula region for each case.

2.3. Drug transport modeling in the vitreous humor

Treatment of inner retinal diseases is challenging due to the ocular anatomical barriers. Four routes can be used for ocular drug delivery in the posterior segment of the eye [38], but our focus

Table 2: Parameter values for Darcy's law

Parameter	Rabbit	Human	Unit	Reference
Density ρ	1000	1008	kg/m^3	[36], [37]
Viscosity μ	0.1 [a]	0.1	Pa·s	[18]
Permeability κ	5.8×10^{-14}	-	m^2	[37]
Permeability/viscosity κ/μ	-	9×10^{-12}	m^2/(Pa·s)	[17]
Inlet u at $z = z_l$	1.5×10^{-7} [a]	1.5×10^{-7}	m/s	[17]
Outflow p at r_v and $z < 0$	0 [a]	0	Pa	[17]

a: Assumed same as human vitreous.

is on intravitreal administration since it is the preferred method of administration. Drug transport in the vitreous is not linearly distributed nor fully understood. Drug distribution in the vitreous depends on human anatomy, eye shape, vitreous properties, and individual ocular topography.

We simulated the administration of the drug bevacizumab in the vitreous humor near the limbus region and observed drug concentration at the vitreous and near the targeted tissue. A typical dose concentration for bevacizumab administration is 1.25mg/0.05mL (about 0.167 mol/m^3) [20, 10, 39], and this concentration is used for both humans and rabbits. The concentration at the injected location is defined as C_i, and the value of the injected drug concentration is $C_i = 0.167$ mol/m^3. The initial drug concentration C_0 in the domain is defined as:

$$C_0 = \begin{cases} C_i & \text{for } (x-x_i)^2 + (y-y_i)^2 + (z-z_i)^2 = r_i^2 \\ 0 & \text{otherwise} \end{cases} \tag{4}$$

where x_i, y_i, and z_i are given in Table 1, and r_i is the resulting radius for a sphere of volume 0.05 mL.

In our study, the PK model captures the continuum of drug movement through the vitreous. We used the transport of diluted species physics in COMSOL to model the mass transport of bevacizumab. The governing equation of drug transport in the vitreous humor is given by

$$\frac{\partial C}{\partial t} = \nabla \cdot (D \nabla C) - u \cdot \nabla C + R \tag{5}$$

where C is the drug concentration, u is the flow velocity, the term $u \cdot \nabla C$ represents the mass transport due to convection, D represents the diffusion coefficient of the drug, R represents the reaction rate, which is zero in our model, and the term $D\nabla C$ describes how much drug diffuses through the vitreous. The drug distribution rate depends on the drug diffusion coefficient value. The diffusion coefficient of the drug bevacizumab in rabbit vitreous humor is $1.2 \pm 0.6 \times 10^{-6}$ cm^2/s [40]. For human vitreous humor, we used the estimated diffusion coefficient value of 9.13×10^{-7} cm^2/s [16]. Table 3 summarizes the parameter values for drug transport in our model.

Table 3: Parameter values for drug transport

Parameter	Rabbit	Human	Unit	Reference
Drug injection concentration C_i	0.167	0.167	mol/m^3	[20, 10, 39]
Drug diffusion coefficient D	1.2×10^{-10}	9.13×10^{-11}	m^2/s	[16, 40]
Reaction rate R	0	0	mol/(m$^3 \cdot$ s)	[24]

For our Case 1, drug transport is governed by both diffusive (random movement due to a concentration gradient ∇c) and convective (AH fluid flow with velocity u as an inlet) effects. In Case 2, we consider the vitreous humor to be stagnant; therefore, convective effects are neglected ($u = 0$).

The major routes of drug elimination are through the aqueous humor drainage (anterior elimination route) and blood-retinal barrier (posterior elimination route), with the anterior elimination route being the predominant one [37]. We considered the hyaloid membrane surface as the anterior elimination route and the outer surface of the vitreous humor as the posterior elimination route. For the boundary conditions in Case a (anterior elimination only) we defined $C = 0$ at the hyaloid membrane's surface in our model. For the boundary conditions in Case b (anterior and posterior elimination) we defined $C = 0$ at the hyaloid membrane's surface and at the vitreous humor's outer surface in our model. By combining the two fluid flow cases in the vitreous with the two cases of drug clearance routes, we estimate the drug time-concentration profile in the vitreous and near the macula region for these four different cases (Case 1a, case 1b, Case 2a, Case 2b).

The concentration on the vitreous humor was calculated as the volume average on the vitreous domain for both rabbit and human. The near the macula concentration for Case 1a and Case 2a was calculated using a point probe at the locations specified on Table 1. For cases 1b and 2b, this method could not be applied given that $C = 0$ is a established boundary conditon. Therefore, using a point probe on the same locations as before we calculated the bevacizumab flux. Using this flux, and surface and volumetric information of the human macula, we calculated a rolling daily average concentration. There is no clearly defined macula in the rabbit eye [41]. Instead, they present a horizontal area with higher cell density called a visual streak [42]. However, we are interested in comparing the amount of drug that is leaving the vitreous humor and reaching the retina near the macula region in both species so we assumed a rabbit "macula" proportional to the scale of a human macula. The human macula has a volume of approximately 8.49 mm^3 [43] and is approximately 5.5 mm in diamater [44]. Table 4 contains the parameters used for the human macula and the rabbit macula approximation.

3. Results and discussion

Our investigation found no other available data except [15] on the computational PK modeling of intravitreal injections using bevacizumab in human and rabbit eyes. Experimental human and rabbit eyes data are available to validate our PK model in vitreous humor. Heljak and

Table 4: Parameter values for human macula and rabbit "macula"

Parameter	Rabbit	Human	Unit	Reference
Diameter	3.84×10^{-3} [a]	5.5×10^{-3}	m	[44]
Volume	2.55×10^{-9} [a]	8.49×10^{-9}	m^3	[43]

a: Values proportional to the scale of a human macula.

Swieszkowski [14] published an *in silico* model of bevacizumab release from PLGA microspheres; however, the reference data shows using properties for fluorescein. Because of the property differences between fluorescein and bevacizumab, we did not consider their results in our model. To validate our computational model, we considered the experimental results of PK studies using WebPlotDigitizer [25] software to collect the data of the drug bevacizumab concentration in vitreous humor in rabbit and human eyes. We found no experimental data that calculates drug concentration in the human macula or the rabbit visual streak region.

3.1. Rabbit eye

Figure 2 shows the time-concentration profile of the drug bevacizumab in the rabbit vitreous humor. We get the slowest clearance in the rabbit eye by considering no convection in the vitreous and anterior elimination only (Case 2a). The fastest clearance from the eye is obtained when considering both anterior and posterior elimination with or without convection (Case 1b and Case 2b, respectively). We get an intermediate clearance when considering convection through the vitreous and anterior elimination only (Case 1a).

Case 2a seems to agree with the experimental data from Bakri et al. [10], but this case overpredicts bevacizumab concentration in the vitreous when compared to the experimental data from the other three studies. Case 1b and Case 2b significantly underestimates drug concentration in the rabbit vitreous compared to the experimental data. Case 1a still underpredicts drug concentration in rabbit vitreous humor, but it is slightly closer to existing experimental data than Case 1b and Case 2b.

It is important to note that the inlet velocity value used in the rabbit simulation is the same as for humans in other studies [17]. Smaller inlet velocity values might be more relevant for rabbits and could help our model be closer to experimental data. Figure 3 shows the velocity profile at the center of the rabbit vitreous.

The anterior elimination route alone cannot sufficiently explain drug clearance in rabbit vitreous humor for most of the data, meaning that posterior elimination also plays a role. These results show that including convection into our model is another way of accounting for "posterior elimination" since the drug is carried out towards the outer surface of the vitreous humor. Results show that in rabbit vitreous humor, the effect of the anterior elimination route is dominant over the posterior elimination route; this is consistent with the results from Lamminsalo et al. [24].

Furthermore, our model results seem to better describe drug concentration in the vitreous after

intravitreal injection for Bakri et al. [10] data when compared to the model by Sibak et al. [15]. One possible reason for this is that they used a bevacizumab diffusion coefficient of 4×10^{-7} cm^2/s, which is significantly lower compared to our value of 1.2×10^{-6} cm^2/s. However, one advantage of our model is the computational simplicity. Their model involved an entire eye geometry with a mesh of 1,526,561 elements, whereas our model involved only the vitreous humor, with proper boundary conditions and a mesh of 185,119 elements.

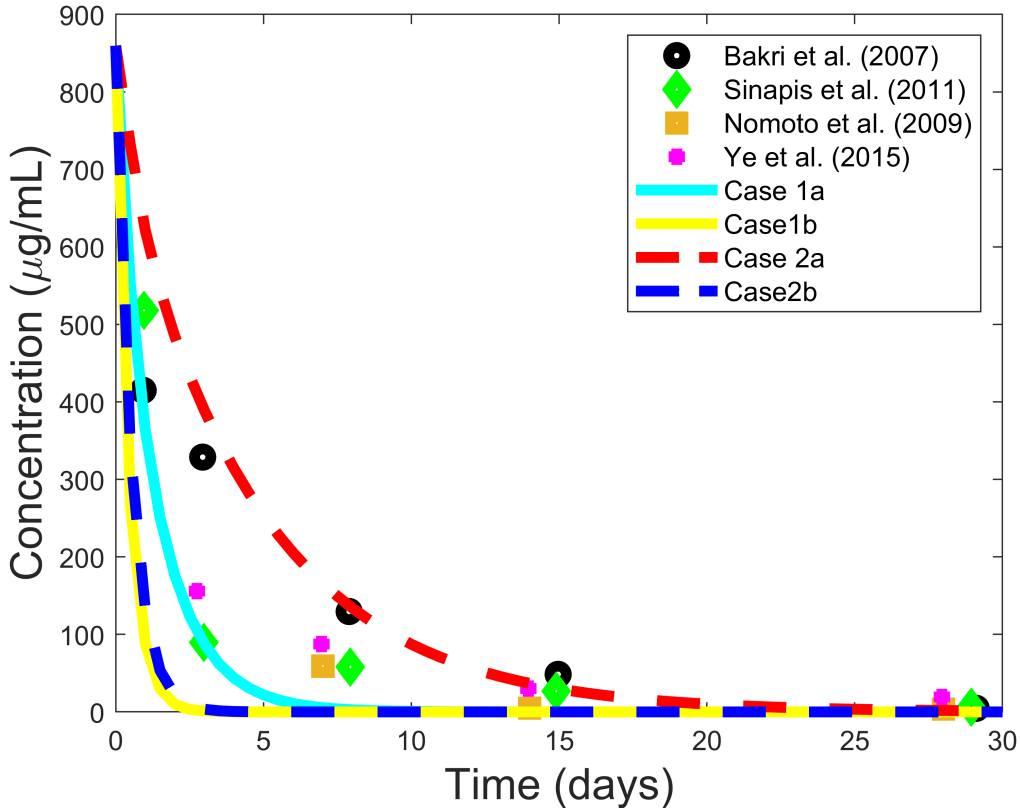

Figure 2: Vitreous humor concentration in the rabbit eye. Experimental (markers) and model results (curves). Case 1a: convective flow with anterior elimination only, Case 1b: convective flow with both anterior and posterior elimination, Case 2a: no convective flow with anterior elimination, and Case 2b: no convective flow with both anterior and posterior elimination. Experimental data from Bakri et al. [10], Sinapis et al. [20], Nomoto et al. [21], and Ye et al. [22].

Figure 4 shows bevacizumab concentration in the rabbit "macula." A minimum concentration of 0.5 μg/mL is required to completely prevent angiogenesis [26]. For Case 1b and Case 2b, bevacizumab concentration goes below the threshold after 6 and 6.5 days, respectively. Case 1a maintains bevacizumab concentration at the macula for about 11.5 days, whereas Case 2a does so for over a month. These results will be compared with bevacizumab concentration in the human

macula since clearance in the human eye is expected to be slower. However, the results are in accordance with the bevacizumab concentration profiles in the vitreous humor obtained in Figure 2.

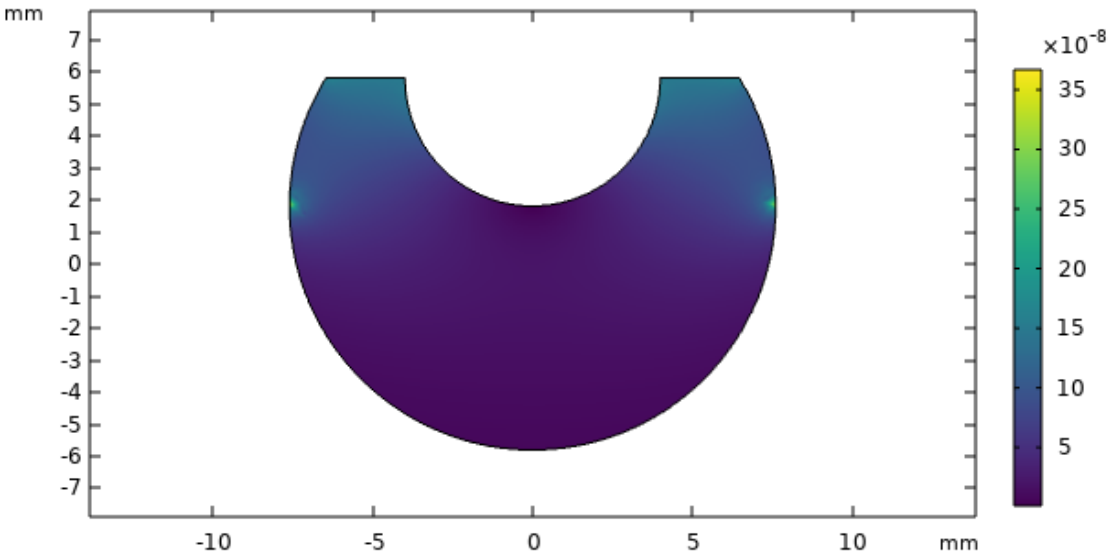

Figure 3: Velocity (m/s) at the center of the rabbit vitreous

3.2. *Human eye*

Figure 5 shows the time-concentration profile of the drug bevacizumab in the human vitreous humor. Similar to the Case for the rabbit vitreous humor, the slowest clearance is when no convective flow and only anterior elimination is considered (Case 2a), followed by convective flow and anterior elimination (Case 1a), then no convection and both anterior and posterior elimination (Case 2b), and the fastest clearance in the eye is obtained when convective flow and both elimination routes are considered (Case 1b).

Case 2a significantly underestimates drug clearance in the eye, and therefore it is clear that the posterior elimination route also plays a significant role in drug clearance from the human vitreous. Case 1a, Case 2b, and Case 1b predict similar results, with Case 1a being the closest to the experimental data. However, Case 1a still overpredicts drug clearance in the eye. Considering a slower velocity in the vitreous humor could help explain experimental data since the extreme case of $C = 0$ with no convection (Case 2b) overpredicts drug clearance in the human vitreous.

In the study by Beer et al. [45], the vitreous humor samples were taken at 48 hours and 4 weeks to measure the drug concentration of bevacizumab for two patients. The drug was injected near the limbus location in the posterior segment of the eye. For patient 1, the drug concentration was found to be 3.33×10^{-12} mol/mL at 4 weeks after the bevacizumab injection. In our computational model, the drug bevacizumab concentration was 1.07×10^{-14} mol/mL within 4 weeks for Case 1a. For patient 2, a concentration of 1.11×10^{-9} mol/mL in the vitreous was found within 48

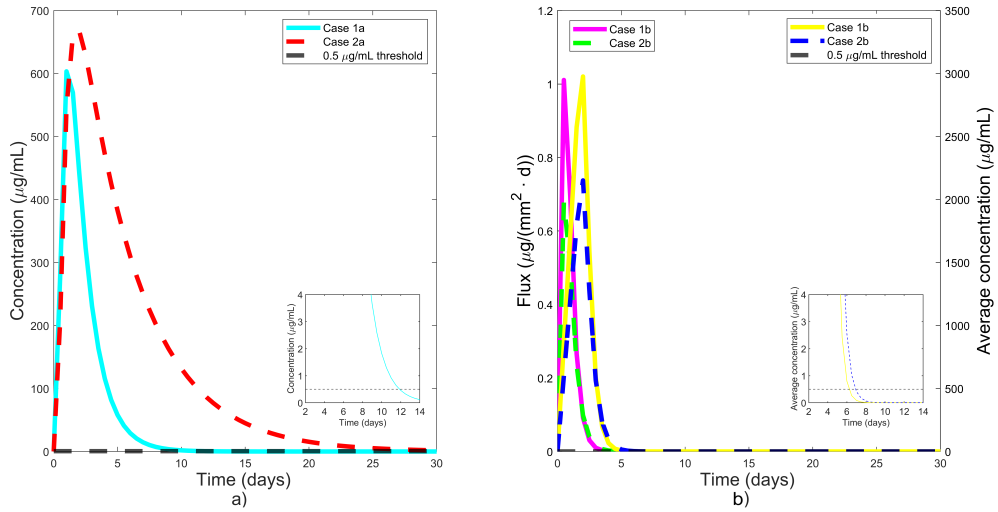

Figure 4: Drug concentration at the rabbit "macula." Case 1a: convective flow with anterior elimination only, Case 1b: convective flow with both anterior and posterior elimination, Case 2a: no convective flow with anterior elimination, and Case 2b: no convective flow with both anterior and posterior elimination

hours, whereas at the same time point in our computational model, we obtained a bevacizumab concentration of 7.75×10^{-10} mol/mL for Case 1a. Case 1a of our current model is accurate during the first few days but then over-predicts bevacizumab clearance at later times. One limitation of our human model is the lack of more available experimental data to better interpret and validate our results. However, compared to rabbit data, the results for human vitreous concentration suggest that the posterior elimination route is more relevant for human vitreous clearance than rabbit vitreous clearance.

Figure 6 shows bevacizumab concentration in the human macula. A minimum concentration of 0.5 μg/mL is required to completely prevent angiogenesis [26]. Case 1b bevacizumab concentration goes below this threshold after 10.5 days, Case 2b takes 15 days to drop its concentration below the threshold, Case 1a takes almost 17.5 days, and Case 2a takes almost 3 months. Intravitreal injections of bevacizumab are usually performed every 4-6 weeks. Therefore, the bevacizumab concentration in the macula is expected to be above the threshold for longer than in Case 1a but less time than in Case 2a. These results for the bevacizumab concentration in the macula are consistent with the bevacizumab vitreous concentration profiles from Figure 5. As expected, these bevacizumab concentration in human macula is maintained above the threshold for longer than for rabbit "macula" since bevacizumab clearance in the rabbit eye is faster than in the human eye.

Khoobyar et al. [17] calculated the pressure plot in the human eye considering the vitreous humor divided into two different regions: a liquefied and a gel-type region. They used different permeability values for each area under Darcy's law to simulate vitreous humor convective flow. They calculated the pressure distribution throughout the vitreous and obtained a maximum pressure

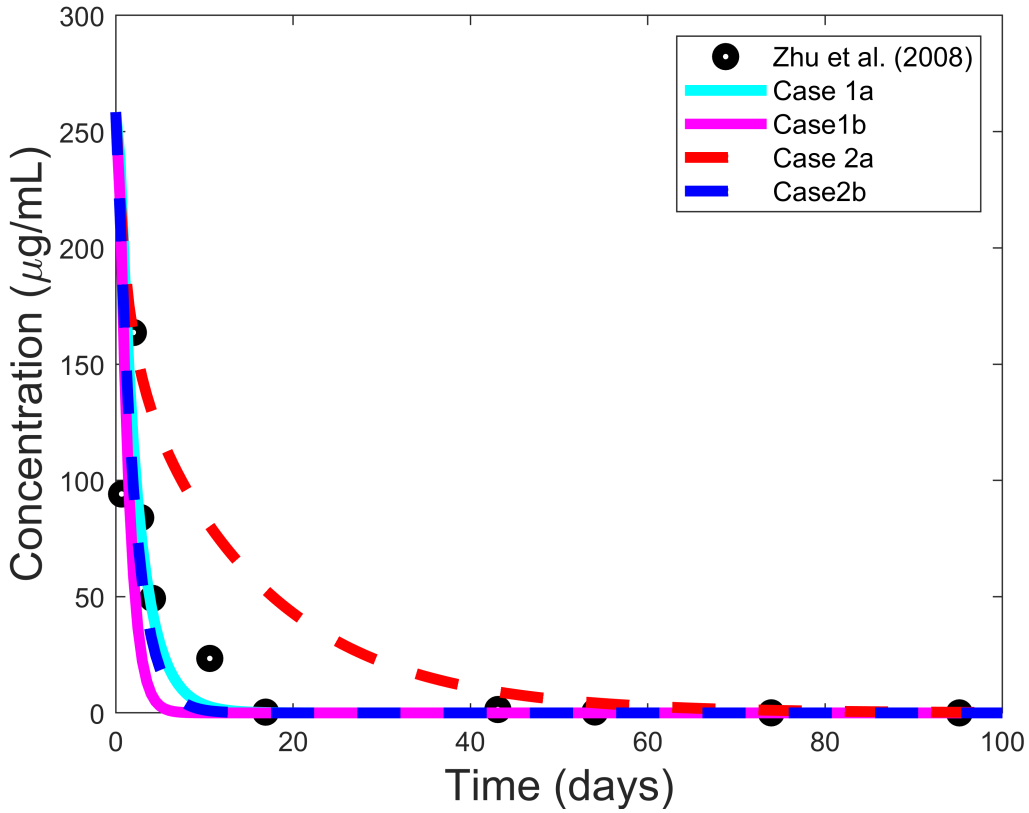

Figure 5: Vitreous humor concentration in the human eye. Experimental (markers) and model results (curves). Case 1a: convective flow with anterior elimination only, Case 1b: convective flow with both anterior and posterior elimination, Case 2a: no convective flow with anterior elimination, and Case 2b: no convective flow with both anterior and posterior elimination. Experimental data from Zhu et al. [23].

of 0.05 kPa [17]. Our model calculated the spatial pressure and velocity in the vitreous domain and found a maximum pressure of above 0.08 kPa (Figure 7) and 25×10^{-8} m/s (Figure 8).

3.3. Conclusions

The drug transport mechanism in the vitreous humor is not entirely understood, and it depends on several factors like anatomy, shape, vitreous properties, and age. Because of these reasons, we have seen differences in the experimental results.

Our PK model can provide a realistic estimate of bevacizumab transport in both human and rabbit eyes. The contribution of computationally implementing the drug concentration-time plot after intravitreal injection in the vitreous and near macula was validated with the experimentally published data. Both our models are in good agreement with the experimental results. The concentration near the macula also showed that the required amount of drug was present in that region

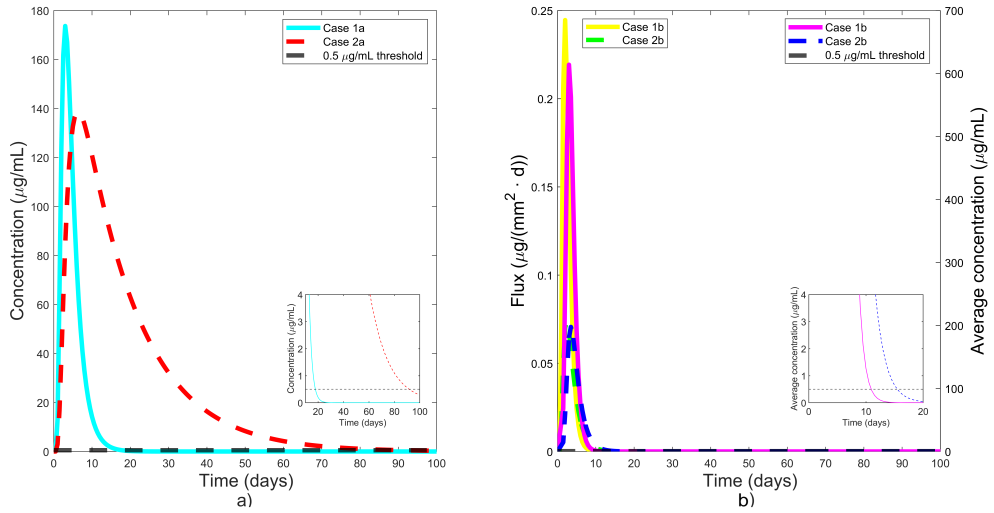

Figure 6: Drug concentration at the human macula. Case 1a: convective flow with anterior elimination only, Case 1b: convective flow with both anterior and posterior elimination, Case 2a: no convective flow with anterior elimination, and Case 2b: no convective flow with both anterior and posterior elimination

to reduce the vascular endothelial growth in the macula for AMD treatment. Our PK model successfully captures the drug absorption and distribution in the vitreous considering the elimination routes from published data. We can use our current PK model for future drug delivery systems using different drugs in AMD treatment to observe the drug kinetics. Our primary goal of this work is to follow similar methods to solve the simulation in both geometries (human and rabbit) to prove that our model can work in relevant preclinical and clinical models using the same techniques.

One limitation of the current work is that it focuses only on intravitreal injection. Others have considered modeling controlled-release drug delivery formulations for intravitreal delivery. Heljak and Swieszkowski [14] considered bevacizumab sustained release from drug-loaded microspheres. Van Kampen et al. [46] considered a hollow hyaluronic acid cylinder intravitreally implanted in the vitreous to observe the drugs Fab and Vitamin B12 release in retinal treatment; a primary focus of the work was to model the drug diffusion coefficients of the implanted hollow cylinder, changing the size (inner and outer radius of the cylinder) so that it could hold the drug for four months. These are directions the current work could be extended towards.

The drug transport in the rabbit eye for the first few days is faster in our model than in other experimental studies. It diffuses faster than other experimental models. The vitreous' physiological and material properties vary a little and are not similar for every vitreous as the drug transport depends on the physiological properties of the vitreous humor, so we have found various concentration profiles for different PK studies done experimentally. Using injection is one of the current treatment processes for AMD, but patient faces frequent amounts of injection as the drug is transported faster in this process. We are trying to implement drug-loaded micro-spheres so that drugs

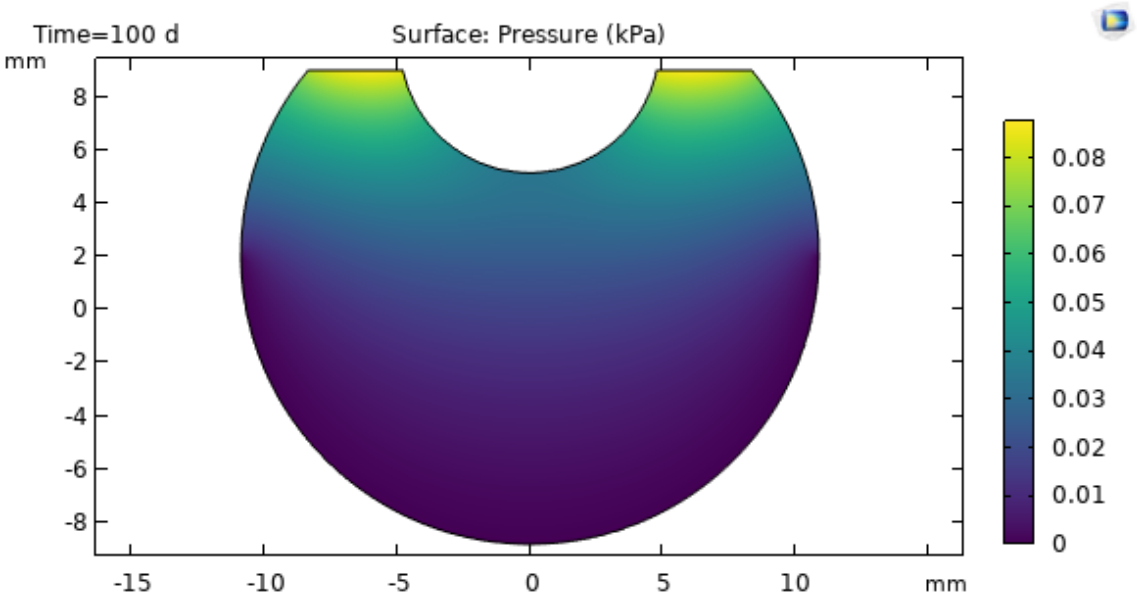

Figure 7: 2D pressure plot in human

can present longer than this injection method in our future work.

Acknowledgments

This work was supported by National Institutes of Health grant R35GM133763 to ANFV, R01EB032870 to KESR and ANFV, Owen Locke Foundation to KESR, and the University at Buffalo. We thank lab members for their thorough feedback on this manuscript and helpful discussions.

References

[1] Pennington KL, DeAngelis MM. Epidemiology of age-related macular degeneration (AMD): Associations with cardiovascular disease phenotypes and lipid factors. Eye Vision. 2016;3:34.

[2] DeAngelis MM, Owen LA, Morrison MA, Morgan DJ, Li M, Shakoor A, et al. Genetics of age-related macular degeneration (AMD). Hum Mol Genet. 2017;26(R1):R45-50.

[3] Rein DB, Wittenborn JS, Zhang X, Honeycutt AA, Lesesne SB, Saaddine J, et al. Forecasting age-related macular degeneration through the year 2050: the potential impact of new treatments. Arch Ophthalmol. 2009;127(4):533-40.

[4] Hadziahmetovic M, Malek G. Age-related macular degeneration revisited: From pathology and cellular stress to potential therapies. Front Cell Dev Biol. 2021;8:612812.

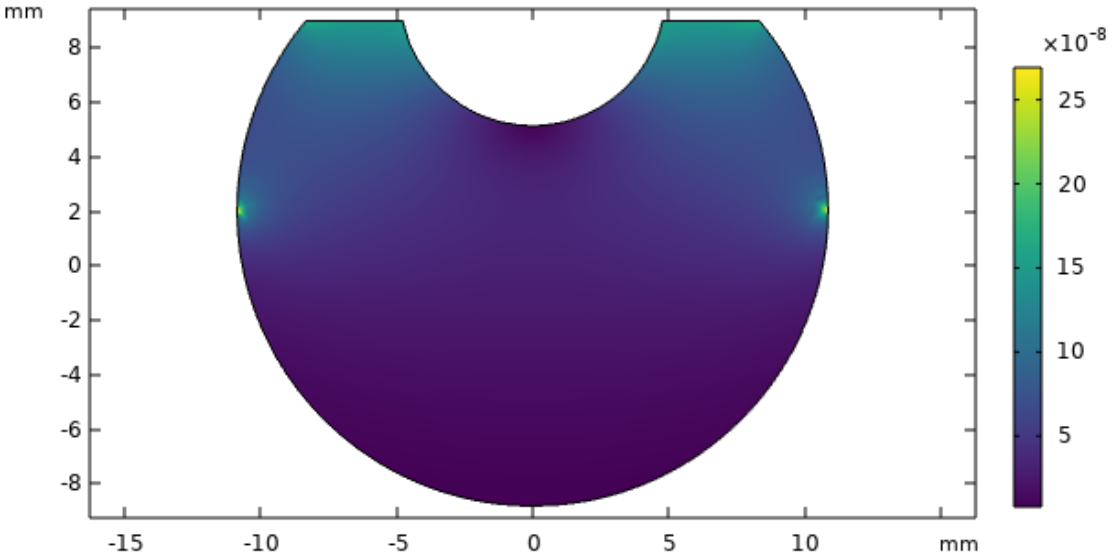

Figure 8: Velocity (m/s) at the center of the human vitreous

[5] Stahl A. The diagnosis and treatment of age-related macular degeneration. Dtsch Arztebl Int. 2020;117(29-30):513.

[6] Rubner R, Li KV, Canto-Soler MV. Progress of clinical therapies for dry age-related macular degeneration. Int J Ophthalmol. 2022;15(1):157.

[7] Serener A, Serte S. Dry and wet age-related macular degeneration classification using OCT images and deep learning. In: 2019 Scientific meeting on electrical-electronics & biomedical engineering and computer science (EBBT). IEEE; 2019. p. 1-4.

[8] Yang S, Zhao J, Sun X. Resistance to anti-VEGF therapy in neovascular age-related macular degeneration: A comprehensive review. Drug Des, Dev Ther. 2016;10:1857.

[9] Varela-Fernandez R, Diaz-Tome V, Luaces-Rodriguez A, Conde-Penedo A, Garcia-Otero X, Luzardo-Alvarez A, et al. Drug delivery to the posterior segment of the eye: Biopharmaceutic and pharmacokinetic considerations. Pharmaceutics. 2020;12(3):269.

[10] Bakri SJ, Snyder MR, Reid JM, Pulido JS, Singh RJ. Pharmacokinetics of intravitreal bevacizumab (Avastin). Ophthalmology. 2007;114(5):855-9.

[11] Del Amo EM, Urtti A. Rabbit as an animal model for intravitreal pharmacokinetics: Clinical predictability and quality of the published data. Exp Eye Res. 2015;137:111-24.

[12] Ahn J, Kim H, Woo SJ, Park JH, Park S, Hwang DJ, et al. Pharmacokinetics of intravitreally injected bevacizumab in vitrectomized eyes. J Ocul Pharmacol Ther. 2013;29(7):612-8.

[13] Chacin Ruiz EA, Swindle-Reilly KE, Ford Versypt AN. Experimental and mathematical approaches for drug delivery for the treatment of wet age-related macular degeneration. J Control Release. 2023;363:464-83.

[14] Heljak MK, Swieszkowski W. In silico model of bevacizumab sustained release from intravitreal administrated PLGA drug-loaded microspheres. Mater Lett. 2022;307:131080.

[15] Sibak MA, Ahmadikia H, Babaee M. Effect of Fluid Flow Direction on Intravitreal Injections of Drugs into Eye. Heat Transfer Eng. 2023.

[16] Hutton-Smith LA, Gaffney EA, Byrne HM, Maini PK, Schwab D, Mazer NA. A mechanistic model of the intravitreal pharmacokinetics of large molecules and the pharmacodynamic suppression of ocular vascular endothelial growth factor levels by ranibizumab in patients with neovascular age-related macular degeneration. Mol Pharmaceutics. 2016;13(9):2941-50.

[17] Khoobyar A, Penkova AN, Humayun MS, Sadhal SS. Mathematical model of macromolecular drug transport in a partially liquefied vitreous humor. J Heat Transfer. 2022;144(3):031208.

[18] Balachandran RK, Barocas VH. Contribution of saccadic motion to intravitreal drug transport: Theoretical analysis. Pharm Res. 2011;28(5):1049-64.

[19] Khoobyar A, Naghdloo A, Penkova AN, Humayun MS, Sadhal SS. Analytical and computational modeling of sustained-release drug implants in the vitreous humor. J Heat Transfer. 2021;143(10):101201.

[20] Sinapis CI, Routsias JG, Sinapis AI, Sinapis DI, Agrogiannis GD, Pantopoulou A, et al. Pharmacokinetics of intravitreal bevacizumab (Avastin®) in rabbits. Clin Ophthalmol. 2011;5:697.

[21] Nomoto H, Shiraga F, Kuno N, Kimura E, Fujii S, Shinomiya K, et al. Pharmacokinetics of bevacizumab after topical, subconjunctival, and intravitreal administration in rabbits. Invest Ophthalmol Visual Sci. 2009;50(10):4807-13.

[22] Ye Z, Ji Y, Ma X, Wen J, Wei W, Huang S. Pharmacokinetics and distributions of bevacizumab by intravitreal injection of bevacizumab-PLGA microspheres in rabbits. Int J Ophthalmol. 2015;8(4):653.

[23] Zhu Q, Ziemssen F, Henke-Fahle S, Tatar O, Szurman P, Aisenbrey S, et al. Vitreous levels of bevacizumab and vascular endothelial growth factor-A in patients with choroidal neovascularization. Ophthalmology. 2008;115(10):1750-5.

[24] Lamminsalo M, Urtti A, Ranta V. Quantitative pharmacokinetic analyses of anterior and posterior elimination routes of intravitreal anti-VEGF macromolecules using published human and rabbit data. Exp Eye Res. 2022;222:109162.

[25] Rohatgi A. WebPlotDigitizer; Version 4.6 Released (September 16, 2022). https://automeris.io/WebPlotDigitizer/.

[26] Varshochian R, Riazi-Esfahani M, Jeddi-Tehrani M, Mahmoudi A, Aghazadeh S, Mahbod M, et al. Albuminated PLGA nanoparticles containing bevacizumab intended for ocular neovascularization treatment. J Biomed Mater Res, Part A. 2015;103(10):3148-56.

[27] Ahn SJ, Hong HK, Na YM, Park SJ, Ahn J, Oh J, et al. Use of Rabbit Eyes in Pharmacokinetic Studies of Intraocular Drugs. J Visualized Exp. 2016;(113).

[28] Azhdam AM, Goldberg RA, Ugradar S. In vivo measurement of the human vitreous chamber volume using computed tomography imaging of 100 eyes. Transl Vision Sci Technol. 2020;9(1):2.

[29] Missel PJ. Simulating intravitreal injections in anatomically accurate models for rabbit, monkey, and human eyes. Pharm Res. 2012;29(12):3251-72.

[30] Mains J, Wilson CG. The vitreous humor as a barrier to nanoparticle distribution. J Ocul Pharmacol Ther. 2013;29(2):143-50.

[31] Zimmerman RL. In vivo measurements of the viscoelasticity of the human vitreous humor. Biophys J. 1980;29(3):539-44.

[32] Tram NK, Swindle-Reilly KE. Rheological properties and age-related changes of the human vitreous humor. Front Bioeng Biotechnol. 2018;6:199.

[33] Haghjou N, Abdekhodaie MJ, Cheng YL, Saadatmand M. Computer modeling of drug distribution after intravitreal administration. Int J Pharmacol Pharm Sci. 2011;5(5):194-204.

[34] Penkova AN, Zhang S, Humayun MS, Fraser S, Moats R, Sadhal SS. Measurement of the hydraulic conductivity of the vitreous humor. J Porous Media. 2020;23(2).

[35] Smith DW, Lee C, Gardiner BS. No flow through the vitreous humor: How strong is the evidence? Prog Retinal Eye Res. 2020;78:100845.

[36] Silva AF, Alves MA, Oliveira MSN. Rheological behaviour of vitreous humour. Rheol Acta. 2017;56:377-86.

[37] Lamminsalo M, Taskinen E, Karvinen T, Subrizi A, Murtomaki L, Urtti A, et al. Extended pharmacokinetic model of the rabbit eye for intravitreal and intracameral injections of macromolecules: Quantitative analysis of anterior and posterior elimination pathways. Pharm Res. 2018;35(8):153.

[38] Balachandran RK. Computational modeling of drug transport in the posterior eye. Ph.D. Dissertation. University of Minnesota. Minneapolis, MN; 2010.

[39] Hård A, Hellström A. On safety, pharmacokinetics and dosage of bevacizumab in ROP treatment–a review. Acta Paediatr. 2011;100(12):1523-7.

[40] Zhang S, Penkova A, Humayun MS, Martinez-Camarillo JC, Tadle AC, Galesic A, et al. In vivo experimental and analytical studies for bevacizumab diffusion coefficient measurement in the rabbit vitreous humor. J Heat Transfer. 2021;143(3).

[41] Pennesi ME, Neuringer M, Courtney RJ. Animal models of age related macular degeneration. Mol Aspects Med. 2012;33(4):487-509.

[42] Penn J, Mihai DM, Washington I. Morphologic and physiologic retinal degeneration induced by intravenous delivery of vitamin A dimers in the leporid retina. Dis Models Mech. 2014;8(2):131-8.

[43] Pokharel A, Shrestha JB, Shrestha GS. Macular thickness and macular volume measurements using spectral domain optical coherence tomography in normal Nepalese eyes. Clin Ophthalmol. 2016:511.

[44] Remington LA. Clinical Anatomy of the Visual System. Saint Louis, UNITED STATES: Elsevier; 2011. Available from: `http://ebookcentral.proquest.com/lib/buffalo/detail.action?docID=1430961`.

[45] Beer PM, Wong SJ, Hammad AM, Falk NS, O'Malley MR, Khan S. Vitreous levels of unbound bevacizumab and unbound vascular endothelial growth factor in two patients. Retina. 2006;26(8):871-6.

[46] Van Kampen E, Vandervelden C, Fakhari A, Qian J, Berkland C, Gehrke SH. Design of hollow hyaluronic acid cylinders for sustained intravitreal protein delivery. J Pharm Sci. 2018;107(9):2354-65.